Paper 188

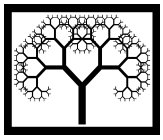

Proceedings of the Eleventh International Conference
on Computational Structures Technology,
B.H.V. Topping, (Editor),
Civil-Comp Press, Stirlingshire, Scotland

Biomechanics of the Willis Circle Arteries

D.V. Ivanov, L.Yu. Kossovich,
Y.E. Salkovsky and N.G. Chernyshevsky
Saratov State University, Saratov, Russia

Abstract

The purpose of the work, described in this paper, was to study the processes of appearance, growth and rupture of aneurysms from a mechanical point of view. A comprehensive study of human Willis circle arteries behaviour was performed. Initially we investigated the mechanical properties of the human Willis circle arteries with the help of uniaxial tensile testing machine Tiratest 28005. According to the results of experiments we determined the parameters of the Mooney-Rivling deformation-energy function, which has been used to describe the behaviour of human Willis circle arteries during further simulations. The constants obtained were utilised in finite element simulation of blood flow through the healthy and pathologically altered human Willis circle arteries. The results of numerical experiments were analysed in order to establish the influence of mechanical factors on the appearance, growth and rupture of the human Willis circle arteries aneurysms.

Keywords: biomechanics, Willis circle arteries, aneurysm, hyperelastic material, Mooney-Rivling, finite element modeling, three-dimensional model.

1 Introduction

Neuron brain functioning requires significant energy expenditure, which brain receives through the vascular system. 4 arteries supply blood to brain – two carotid and two vertebral. These arteries carry about 20 % of all the human blood flow. In the cranium, the internal carotid artery (ICA) grows into anterior cerebral artery (ACA) and middle cerebral artery (MCA). Vertebral arteries (VA) merge into basilar artery (BA) which grows into two posterior cerebral arteries (PCA). These three pares of cerebral arteries (anterior, middle and posterior) form a circle of Willis (COW) [1-3]: anterior cerebral arteries unite with anterior communicating artery (ACoA), between middle and posterior cerebral arteries there is a posterior

communicating artery (PCoA). Such “normal structure of COW” can be found in 25 % of all cases.
One of the most dangerous and frequent diseases of COW arteries are aneurisms [4] (local dilatation of arteries). The most frequent aneurism localizations are artery bifurcations: the place of carotid artery division into ACA and MCA, the place of ACA and ACoA connection, the place of ICA and PCoA connection. Sometimes there are aneurisms of brain foundation vessels. If aneurism ruptures, blood can penetrate into gray matter and clinical syndrome of ventricular hemorrhage can appear.
Modern investigations allowed proving the existence of inborn, acquired and inherited defects of arterial wall [5]. The aneurisms mostly appear because of hemodynamic and moronic damages of arterial wall. It is considered that prevalence, growth, thrombus presence and aneurism rupture may be explained by means of the hemodynamic theory [5]. Thereby there is a necessity in exposure of mechanical factors of aneurism appearance and development. So it is necessary to simulate blood flow through the COW. This needs to know mechanical properties of arteries walls.
The purpose of this study is to identify the hemodynamic and mechanical factors affecting growth, development and rupture of aneurysms. The study was carried out for several stages. At the first stage the mechanical properties of the Willis circle arteries were identified. Then the geometric models of Willis circle arteries were constructed. Then boundary value problems of blood flow through the arteries with rigid and flexible walls were solved with the help of finite element method. Numerical results were processed and analyzed.

2 Analysis

2.1 Mechanical experiments

In our experiments we used uniaxial tensile testing machine TiraTest 28005 (registration number 23512-02 in the State Register of the Russian Federation) with 100N load cell. The values of the applied force (H) and stretch (mm) in the application of force direction were recorded in the course of the experiment.
All the samples of vessels were divided into two gender groups and into four age groups (see Table 1, age of death 22-90 corresponds to four age groups for male and female).

Age group number	Age, years	
	Male	Female
1	22-35	21-35
2	36-60	36-55
3	61-74	56-74
4	75-90	75-90

Table 1: Age and gender groups

Experimental data processing showed age changes and gender differences of vessels material. Diagram stress-lengthening degree is highly non-linear (Figure 1).

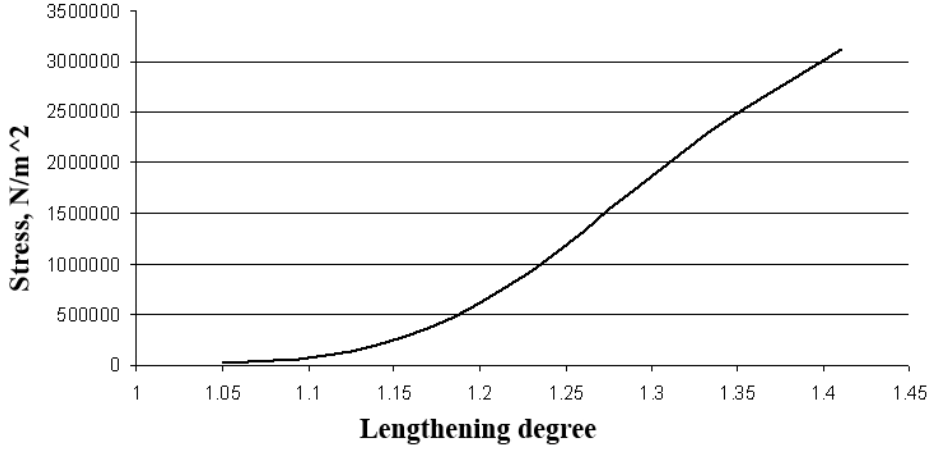

Figure 1. Diagram stress-lengthening degree.

Ultimate tensile strength in longitudinal direction decreases during lifetime. The greatest difference between the ultimate tensile strength for the 1 and 4 age groups was found for the basilar artery, and it is about 50%. For the rest of the arteries the difference is not more than 30-40%.

The influence of gender significantly affects the strength characteristics of the arteries. Ultimate tensile strength in the longitudinal direction of the arteries taken from female is 1.1-1.3 times less than that of men. The greatest difference between the ultimate tensile strength in the longitudinal direction was found for the vertebral arteries. Ultimate tensile strength of the vertebral arteries was maximal for both women and men.

Deformability of all arteries reduces with age. In the longitudinal direction walls of the vertebral and middle cerebral arteries have the highest deformability compared with other arteries. The lowest deformability was detected for the cerebellar artery wall.

Results of the mechanical experiments were used for obtaining the constants of hyperelastic rubber-like Mooney-Rivlin material. For example we considered the basilar artery and obtained constants for this artery. We derived the relationship between stress and the degree of elongation in uniaxial tension with strain energy function.

2.2 Obtaining Mooney-Rivling parameters

Consider right and left Cauchy-Green deformation tensors $C = F^T F$, $B = FF^T$ respectively, where F is the gradient deformation tensor. Invariants of right tensor (similarly for left tensor) are determined using $I_1 = tr(C)$, $I_2 = \frac{1}{2}\left(I_1^2 - tr\left(C^2\right)\right)$, $I_3 = \det(C)$. Material of the arteries walls is considered to be incompressible [6],

therefore $I_3 = 1$. Gradient deformation tensor can be written in matrix form $F = \begin{pmatrix} \lambda_1 & 0 & 0 \\ 0 & \lambda_2 & 0 \\ 0 & 0 & \lambda_3 \end{pmatrix}$, where $\lambda_1, \lambda_2, \lambda_3$ are the lengthening rates. In this case right and left Cauchy-Green deformation tensors coincide and $C = B = F^2 = \begin{pmatrix} \lambda_1^2 & 0 & 0 \\ 0 & \lambda_2^2 & 0 \\ 0 & 0 & \lambda_3^2 \end{pmatrix}$. Invariants of tensor C are defined by the next expressions

$$I_1 = \lambda_1^2 + \lambda_2^2 + \lambda_3^2,$$
$$I_2 = \frac{1}{2}\left(I_1^2 - tr\left(C^2\right)\right) = \frac{1}{\lambda_1^2} + \frac{1}{\lambda_2^2} + \frac{1}{\lambda_3^2},$$
$$I_3 = \det(C) = \det\left(F^2\right) = \left(\lambda_1\lambda_2\lambda_3\right)^2 = 1.$$

Expression for stresses in the stretched sample are defined by $\sigma_{ii} = \lambda_i^2\Phi - \frac{1}{\lambda_i^2}\Psi + p,$ where $\Phi = 2\frac{\partial W}{\partial I_1}, \Psi = 2\frac{\partial W}{\partial I_2}$ [7] (for the incompressible material strain energy function depends on the two first invariants $W = W\left(I_1, I_2\right)$).

In the case of uniaxial tension $\sigma_{11} \neq 0, \sigma_{22} = \sigma_{33} = 0$. From the equality $\sigma_{33} = 0$ we can derive $\lambda_3^2\Phi - \frac{1}{\lambda_3^2}\Psi + p = 0, \quad p = \frac{1}{\lambda_3^2}\Psi - \lambda_3^2\Phi$. Substitute this derived p into σ_{11}, σ_{22}.

$$\sigma_{11} = \lambda_1^2\Phi - \frac{1}{\lambda_1^2}\Psi + \frac{1}{\lambda_3^2}\Psi - \lambda_3^2\Phi = \left(\lambda_1^2 - \lambda_3^2\right)\Phi - \left(\frac{1}{\lambda_1^2} - \frac{1}{\lambda_3^2}\right)\Psi,$$
$$\sigma_{22} = \lambda_2^2\Phi - \frac{1}{\lambda_2^2}\Psi + \frac{1}{\lambda_3^2}\Psi - \lambda_3^2\Phi = \left(\lambda_2^2 - \lambda_3^2\right)\Phi - \left(\frac{1}{\lambda_2^2} - \frac{1}{\lambda_3^2}\right)\Psi.$$

Taking to consideration incompressibility ($\lambda_3 = \frac{1}{\lambda_1\lambda_2}$), we obtain

$$\sigma_{11} = \left(\lambda_1^2 - \frac{1}{\lambda_1^2\lambda_2^2}\right)\Phi - \left(\frac{1}{\lambda_1^2} - \lambda_1^2\lambda_2^2\right)\Psi,$$
$$\sigma_{22} = \left(\lambda_2^2 - \frac{1}{\lambda_1^2\lambda_2^2}\right)\Phi - \left(\frac{1}{\lambda_2^2} - \lambda_1^2\lambda_2^2\right)\Psi = \left(\lambda_2^2 - \frac{1}{\lambda_1^2\lambda_2^2}\right)\left(\Phi + \lambda_1^2\Psi\right).$$

Taking into account that $\sigma_{22} = 0,$ we have $\lambda_2^2 - \frac{1}{\lambda_1^2\lambda_2^2} = 0 \Leftrightarrow \lambda_2^4 = \frac{1}{\lambda_1^2} \Leftrightarrow$

$\Leftrightarrow \lambda_2^2 = \frac{1}{\lambda_1}.$

Then (designating $\lambda_1 = \lambda$)

$$\sigma_{11} = \left(\lambda^2 - \frac{1}{\lambda^2 \frac{1}{\lambda}} \right) \Phi - \left(\frac{1}{\lambda^2} - \lambda^2 \frac{1}{\lambda} \right) \Psi = \left(\lambda^2 - \frac{1}{\lambda} \right) \Phi - \left(\frac{1}{\lambda^2} - \lambda \right) \Psi =$$

$$= \left(\lambda^2 - \frac{1}{\lambda} \right) \left(\Phi + \frac{1}{\lambda} \Psi \right).$$

Tensor invariants will take a form $I_1 = \lambda^2 + \frac{2}{\lambda}, \; I_2 = \frac{1}{\lambda^2} + 2\lambda.$ Finally, we obtain the stress-strain dependence in case of uniaxial tension $\sigma = 2\left(\lambda^2 - \frac{1}{\lambda} \right) \left(\frac{\partial W}{\partial I_1} + \frac{1}{\lambda} \frac{\partial W}{\partial I_2} \right),$

where $\lambda = \frac{l}{l_0}$ – lengthening degree.

Consider the Mooney-Rivling strain energy function

$$W = C_1 (I_1 - 3) + C_2 (I_2 - 3) \text{ [7].}$$

Then

$$\sigma = 2\left(\lambda^2 - \frac{1}{\lambda} \right) C_1 + 2\left(\lambda - \frac{1}{\lambda^2} \right) C_2. \qquad (1)$$

Thus, having this dependence and results of material uniaxial testing, one can found strain energy function coefficients with the help of the least squares method.

Figure 2 shows the following curves: the dotted line is the ($\sigma - \lambda$) dependence, made from the interpolated experimental data, solid line is the ($\sigma - \lambda$) dependence, obtained from formula (1) with the found constants $C_1 = 5.2 \; N/m^2, \; C_2 = -5.54 \, N/m^2.$

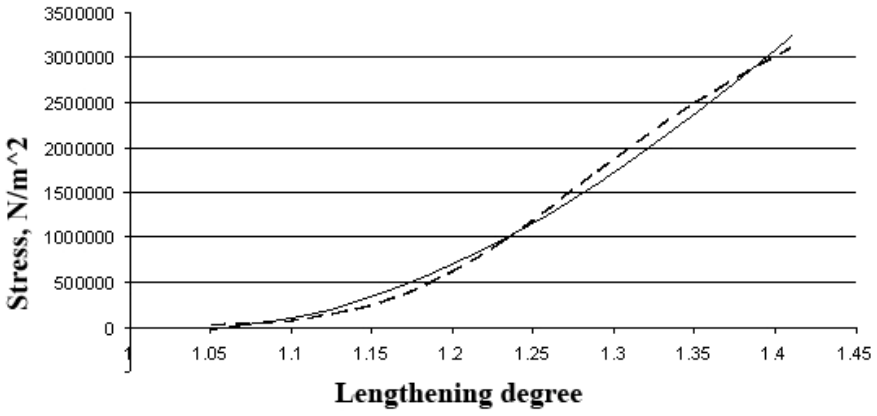

Figure 2. Diagrams ($\sigma - \lambda$). Solid line solid line is the ($\sigma - \lambda$) dependence, obtained from the formula (1), dotted – experimental data.

As seen from Figure 4, difference between experimental (dotted) and theoretical (solid) curves is not significant.

2.3 Finite-element simulations

Results are presented in the article in an agreement with the growth of the complexity of the problem mathematical formulation: blood flow through arteries with rigid walls, the blood flow through the arteries with a flexible walls and the problem of locally weakened artery wall loaded with internal pressure. In the first case we solved the problem of the blood flow in the vessels with simplified geometric models with small and large aneurisms. We used the symmetric and asymmetric boundary conditions at the outlets. In the second case we had a complicated problem formulation - the geometry of vascular models was as close as possible to the real, the walls were assumed to be hyperelastic. The third type of the problem is a boundary-value problem with three-dimensional formulations and a simplified geometry of blood vessel with locally weakened wall. As a model of the wall material, we used perfectly elastic and hyperelastic materials.
In our simulations were had the following assumptions. Blood was considered as a homogeneous viscous incompressible Newtonian fluid with constant density 1050 kg/m^3 and dynamic viscosity 0.004 Pa s. The density of the vessel wall was 1378 kg/m^3. At the entrance of the vessel we set blood pressure, which varies according to physiological law.
For velocities of blood at the outlets of the posterior cerebral artery we chose two types of boundary conditions - symmetrical and asymmetrical. Symmetry was for the equality of average linear velocity at the outlets and the asymmetry - in their relationship from 0.35 to 0.65. We used asymmetric boundary conditions in order to study the flow of blood in the aneurysm in the presence of asymmetric blood flow in the vessel. Changing the speed in time also corresponded to the physiological law. The boundary conditions for pressure and velocity were taken from the literature [8]. The initial conditions for the nonstationary problem were obtained by solving the steady-state problem.

3 Results and discussion

3.1 Simplified geometric models of the basilar artery bifurcation with aneurysms

Figures 3-6 demonstrate shear stress distribution and the pressure fields on the wall of a three-dimensional model of the basilar artery bifurcation with a small and a large aneurysms with symmetric and asymmetric boundary conditions at the outlets. Tangential stress on the arterial wall reaches the minimum value (< 1.5 Pa) on the wall of the aneurysm for both cases of symmetric and asymmetric boundary conditions. These results are similar to those obtained in [9]. In accordance to the theory presented in [10], low values of shear stress lead to deposition of lipids and, consequently, the formation of atherosclerotic plaques and rupture of aneurysms [11].

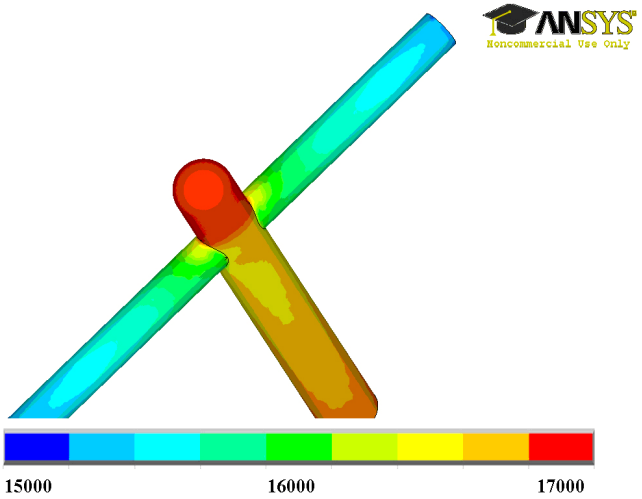

Figure 3. Pressure field for three-dimensional model of the basilar artery bifurcation with small aneurysm.

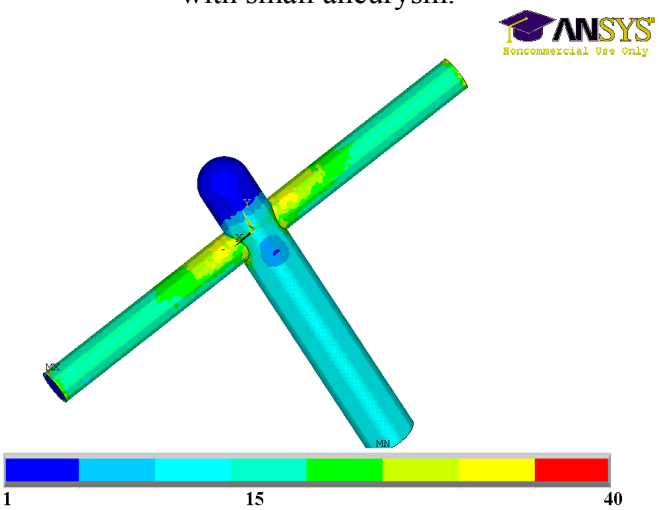

Figure 4. Shear stress field for three-dimensional model of the basilar artery bifurcation with small aneurysm.

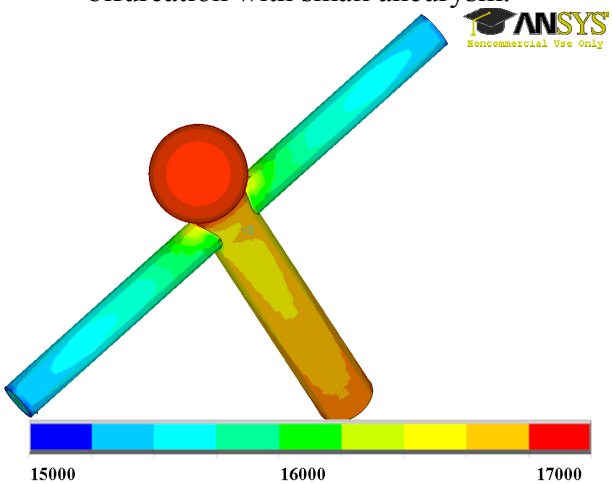

Figure 5. Pressure field for three-dimensional model of the basilar artery bifurcation with big aneurysm.

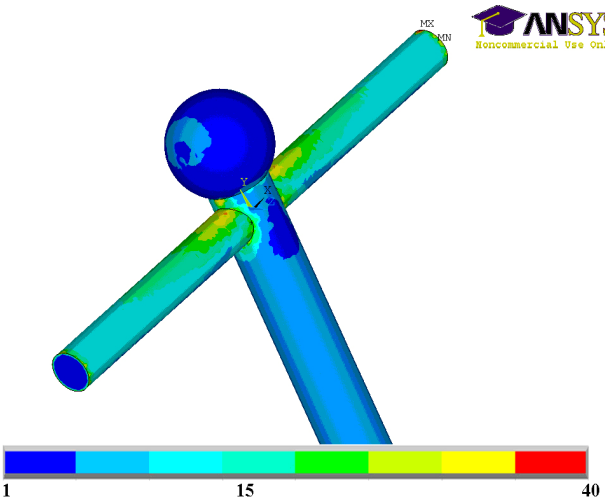

Figure 6. Shear stress field for three-dimensional model of the basilar artery bifurcation with big aneurysm.

Numerical experiments showed that the maximum blood pressure appeared in the aneurysm, therefore a weakened wall of the aneurysm may rupture in the dome [12-15].

For further analysis of the blood pressure effect on the tension of the aneurysm wall, we use the Laplace low

$$T = pR \quad \text{(tension of the wall of a cylindrical shell)}, \qquad (2)$$

$$T = \frac{pR}{2} \quad \text{(tension of the wall of a spherical shell)}, \qquad (3)$$

where T – is tension of the wall in a thin-walled shell, p – internal pressure, R - radius of curvature of the shell.

Formulas (2) and (3) determine the tension in the thin shell across its radius and internal pressure. At the same pressures and radii, tension of spherical aneurysm wall is twice smaller than tension of the cylindrical aneurysm. Calculations showed that the pressures in the dome were almost identical (difference less than 1%). The ratio of the radii of the spherical and cylindrical aneurysms was equal to 1.5. So we can conclude that the probability of cylindrical aneurysm rupture is more than spherical. Similar conclusions are presented in [16, 17].

According to the results of numerical experiments, we have constructed graphs of the linear velocity of blood flow in the neck of the aneurysm in the case of symmetric (Figure 7) and asymmetric (Figure 8) boundary conditions.

Figure 3 shows the symmetric profile of the velocity in the neck of the aneurism and Figure 4 demonstrates an asymmetric profile of the velocity in the neck of the aneurism. The maximum values of linear velocity are related as 1 to 8 respectively. The increase of flow velocity in the case of asymmetric boundary conditions indicates a larger kinetic energy flux and, consequently, an increase of hemodynamic load on the wall of the aneurysm. The increased load on the wall can lead to more rapid growth or rupture.

Figure 7. Profile of the linear velocity in the neck of the aneurism in case of symmetric boundary conditions.

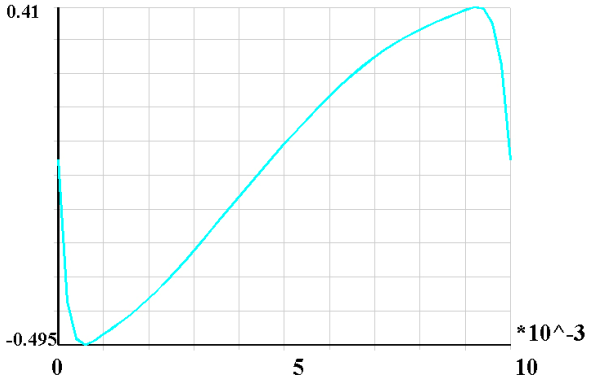

Figure 8. Profile of the linear velocity in the neck of the aneurism in case of asymmetric boundary conditions.

Also we can note relation between vortexes in the dome of the aneurysm (Figures 9, 10) and zones of low shear stress at the wall and, as was shown in [18] based on a comparison of computer tomography and numerical data, with zones of atherosclerotic plaques in the aneurysm.

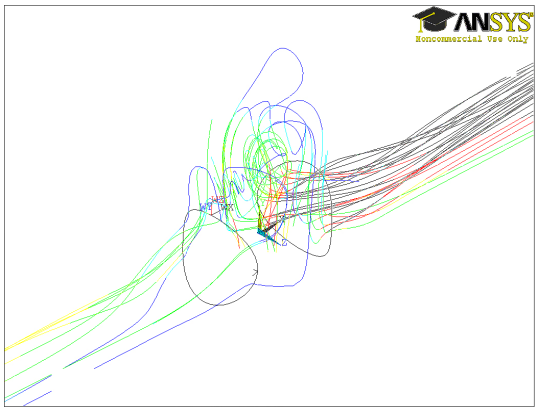

Figure 9. Vortexes in the dome of the small aneurism.

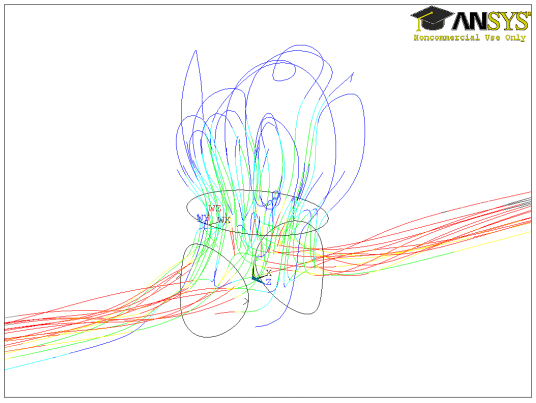

Figure 10. Vortexes in the dome of the big aneurism.

3.2 Three-dimensional models of the arteries without aneurysm with flexible walls

Concentration of shear stress and von Mises equivalent stress on the Figures 11, 12 in the area of apex may lead to the destruction of the media layer, and elastin fibers and, consequently, the formation of aneurysms in this area.

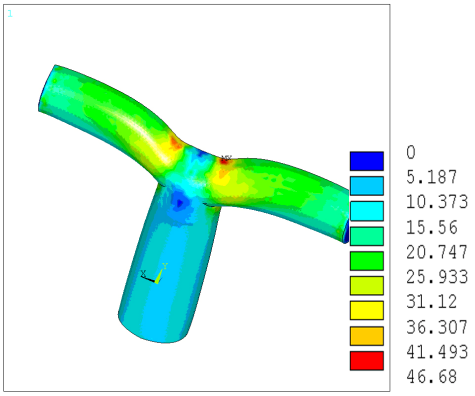

Figure 11. Shear stress field on the wall of a three-dimensional model of basilar artery bifurcation without aneurysm.

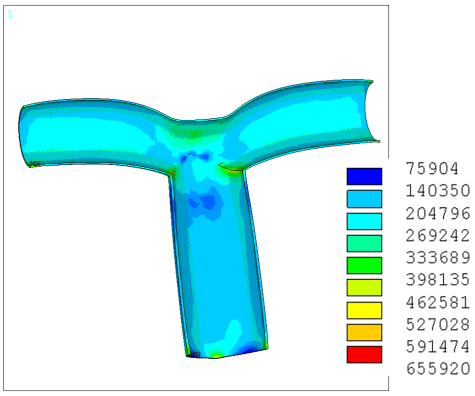

Figure 12. Effective von Mises stress field in the wall of a three-dimensional model of basilar artery bifurcation without aneurysm.

This was confirmed by researchers in [19-22]. It was also found that blood pressure in the apex of bifurcation takes maximum values during the all cardiac cycle, which can also cause weakening of the wall and the growth in the zone apex aneurysms [12, 13].
Similarly, for a model of a closed circle of Willis, the high concentration of von Mises equivalent stress Figures 13-15 coincides with the zones of the most probable formation of aneurysms [23] - bifurcation of the basilar artery, the bifurcation of the middle cerebral and anterior cerebral, anterior cerebral and anterior communicating arteries.
Zones of low shear stress at the wall of the anterior communicating artery (see Figure 16) coincide with zones of deposition of atherosclerosis [23].

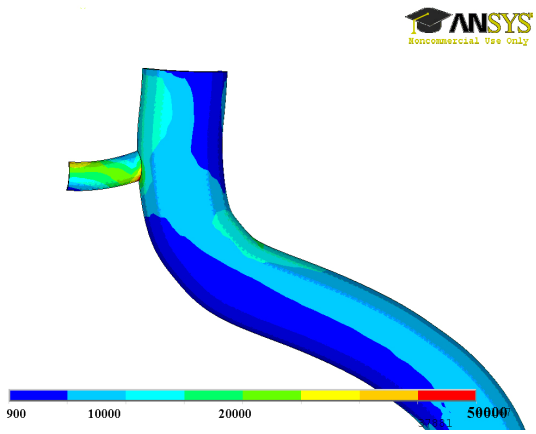

Figure 13. Effective von Mises stress field in the wall of a three-dimensional model of anterior cerebral artery bifurcation without aneurysm (closed circle of Willis).

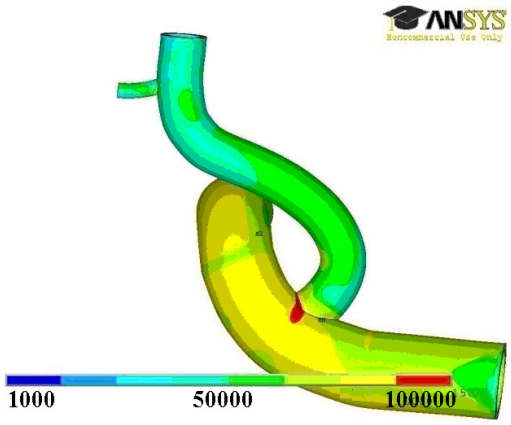

Figure 14. Effective von Mises stress field in the wall of a three-dimensional model of middle cerebral artery bifurcation without aneurysm (closed circle of Willis).

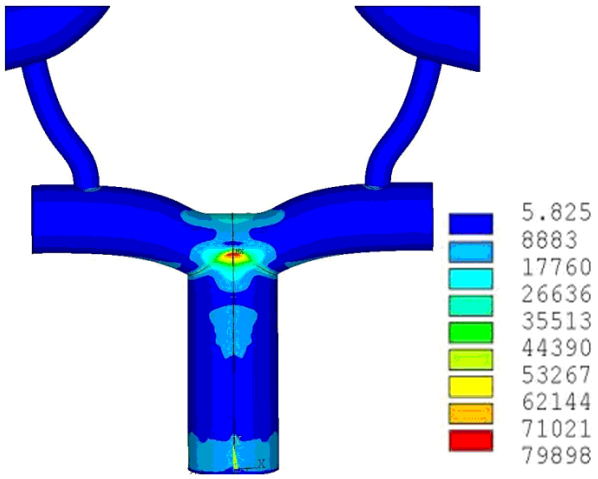

Figure 15. Effective von Mises stress field in the wall of a three-dimensional model of basilar artery bifurcation without aneurysm (closed circle of Willis).

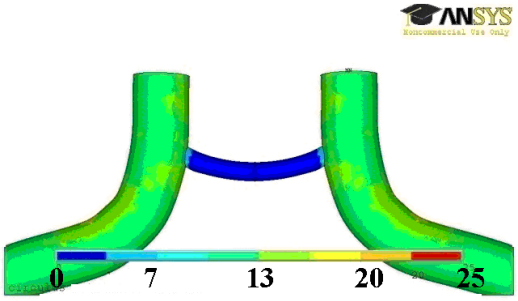

Figure 16. Shear stress field on the wall of a fragment of three-dimensional model of the real human circle of Willis without aneurism.

3.3 Models of locally weakened artery wall

Consider a simplified model of a locally weakened artery. The wall was loaded with internal pressure which magnitude varied in the physiological range.
In the first case, the arterial wall material was assumed to be perfectly elastic, the weakened section of the wall was simulated by reducing the Young's modulus of the material. In the second case the wall was assumed to be hyperelastic. For the weakened area we used a more flat curve than for the healthy area i.e. at the same deformation weakened wall has smaller stress compared to the one for the healthy wall.
This model illustrates the process of aneurysm appearing at the site of the weakened wall. Figure 17 shows the result of this process in three-dimensional model, as in Figure 18 - in two dimensions. For comparison with the healthy wall on Figure 19 we showed results of calculation with the same load as in the case, shown in Figure 18. Comparison of Figures 17 and 18 shows that in the case of locally weakened wall strains on the affected area are larger than deformations in the case of a completely healthy artery. This simulation allows demonstrating the initial stage of development of the aneurysm, in which the wall is only deformed.

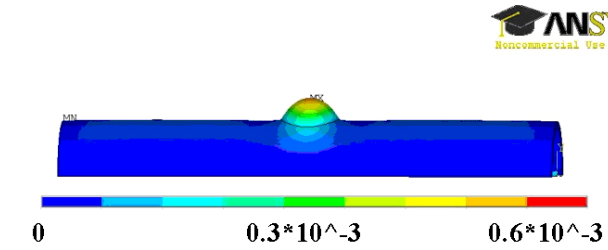

Figure 17. Deformations of a simplified three-dimensional model of locally weakened artery loaded with internal pressure.

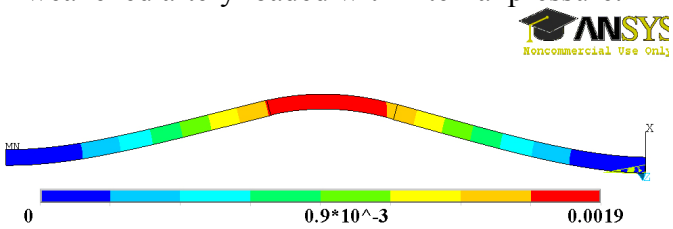

Figure18. Deformations of a simplified two-dimensional model of locally weakened artery loaded with internal pressure.

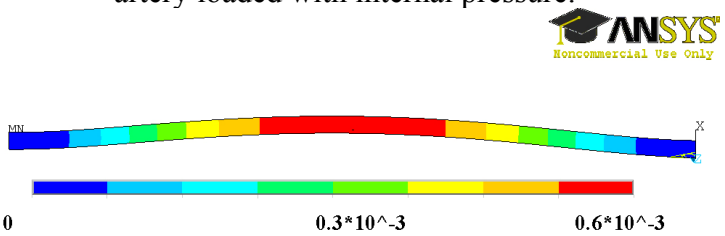

Figure 19. Deformations of a simplified two-dimensional model of healthy artery loaded with internal pressure.

4 Conclusions

This paper presents the results of solving the complex problem, solution of which is aimed at explaining the mechanical point of view on the processes of formation and growth of aneurysms. We consider several models of arteries with and without aneurysms in productions with rigid and flexible walls. The hyperelastic parameters of the model wall used in the numerical calculations were obtained from the results of uniaxial tensile experiments human artery walls.

The numerical results were analysed in terms of the influence of mechanical and hemodynamic factors on the appearing and development of aneurysms in cerebral arteries of the circle of Willis. We found that high values of blood pressure in the apex bifurcation of the arteries can lead to aneurism growth. Concentrations of high shear stress and equivalent stress of von Mises can cause degenerative damage to the wall and provoke its weakening and, consequently, the growth of the aneurysm. It was shown that the more elongated cylindrical aneurysms are more prone to rupture than the spherical of the same radius.

Vortices in the aneurysm correlate with zones of low shear stress (< 1.5 Pa) which indicate the presence of atherosclerotic plaques on the aneurysm wall. An aneurysm in two-dimensional and three-dimensional simplified models of the artery wall was mathematically modelled and illustrated at its initial stage of formation.

References

[1] Luzga, D., Roentgen of vascular system anatomy, Budapest, 380 p., 1968.
[2] Belenkaya, R.M., Stroke and variants of cerebral arteries, Moscow, Medicine, 176 p., 1979.
[3] Gindtse, B.K., Cerebrovascular system human being and animals, Moscow, Medgiz, 95 p., 1947.
[4] Krylov, V.V., Tkachev, V.V., Dobrovolsky G.F., Microsurgery of aneurisms of polygon of Willis, Moscow, 160 p, 2004.
[5] The Federal Centre of pain surgery: www.brainport.ru.
[6] Carew, T.E., Vaishnav, R.N., Pater D.J., Compressibility and Constitutive Equation for Arterial Wall, Circ. Res. 1968. - V. 23. - P. 61-68.
[7] Green, A., Adkins, G., Large deformations and nonlinear mechanics of continuum, Moscow, 456 p., 1965.
[8] Valencia, A. Simulation of unsteady laminar flow in models of terminal aneurysm of the basilar artery / A. Valencia // Int. J. of CFD. – 2005. – Vol. 19, Issue 4. – P. 337-345.
[9] Numerical validation of mr-measurement-integrated simulation of blood flow in a cerebral aneurysm / K. Funamoto [et al.] // Annals of biomedical engineering, 2009. – Vol. 37, № 6. – P. 1105-1116.
[10] Malek, A.M. Hemodynamic shear stress and its role in atherosclerosis / A.M. Malek, S.L. Alper, S. Izumo // J. of the American Medical Association. – 1999. Vol. – 282. – P. 2035–2042.
[11] Lee, Y. Hemodynamics of a cerebral aneurysm model / Y. Lee // California engineer student journal of the UC engineering colleges. – 2006. – P. 20-23.
[12] Carmihael, R. Gross defects in the mascular and elastic coats of the lager cerebral arteries / R. Carmihael // J. of Pathology and Bacteriology. – 1945. – Vol. 57– P. 345-351.
[13] Crowford, T. Some observations on the pathogenesis and natural history of intracranial aneurysms / T. Crowford // J. of Neurology, Neurosurgery & Psychiatry. – 1959. – Vol. 22. – P. 259-266.
[14] Coupe, N., R. Athwal, L. Marshman, and H. Brydon. Subarachnoid hemorrhage emanating from a ruptured infundibulum case report and literature review. Surg. Neurol. 67:204–206, 2007.
[15] Cowan, J. A., G. Barkhoudarian, L. J. Yang, and G. B. Thompson. Progression of a posterior communicating artery infundibulum into an aneurysm in a patient with alagille syndrome. J. Neurosurg. 101:694–696, 2004.
[16] Effects of size and shape (aspect ratio) on the hemodynamics of saccular aneurysms: a possible index for surgical treatment of intracranial aneurysms / H. Ujiie [et al.] // J. of Neurosurgery. – 1989. – Vol. 45. – P. 119-129.
[17] Oshima, M. A new approach to cerebral hemodynamics / M.A. Oshima // Bulletin for The International Association for Computational Mechanics. – 2004. –Vol. 16, Issue 4. – P. 4-9.
[18] Numerical modeling of the flow in intracranial aneurysms: prediction of regions prone to thrombus formation / V.L. Rayz [et al.] // Annals of biomedical engineering. – 2008. – Vol. 36. – P. 1793–1804.

[19] Kondo, S. Cerebral aneurysms arising at nonbranching sites. An experimental study / S. Kondo [et al.] // Stroke. – 1997/ – Vol. 28. – P. 398-403.
[20] Three-dimensional blood flow analysis in a wide-necked internal carotid artery-ophthalmic artery aneurysm. / S Tateshima [et al.] // J. Of Neurosurgery. – 2003. – Vol. 99. – P. 526–533.
[21] Fluid-structure interaction modeling of aneurismal conditions with high and normal blood pressures / R. Torii [et al.] // Computational Mechanics. – 2006. – Vol. 38. – P. 482-490.
[22] Sforza, D., C. Putman, and J. Cebral. Hemodynamics of cerebral aneurysms // Annu. Rev. Fluid Mech. --2009. -- Vol. 41. -- P. 91-107.
[23] Thubrikar, M.J. Vascular mechanics and pathology / M.J. Thubrikar. – New York : Springer Science+Business media, 2007. – 494 p.